5TH BRAZILIAN MRS MEETING

Electron beam effects on amorphous molybdenum oxide nanostructures grown by condensation in hydrogen

Donovan E. Diaz-Droguett · Victor M. Fuenzalida · Marcela S. Diaz-Espinoza · Guillermo Solorzano

Abstract Molybdenum trioxide (MoO$_3$) was evaporated from a tungsten resistive source in presence of hydrogen as carrier gas at pressures from 100 Pa to 600 Pa. Crystalline samples of molybdenum oxide were obtained at source temperatures below 950 °C. However, at source temperatures above 1000 °C, nanoporous structures were obtained, with porosity in the range of 10–85 nm. As shown by X-ray diffraction as well as selected area electron diffraction (SAED), the nanoporous material was amorphous. Under transmission electron microscopy (TEM) examination, and due to the electron beam, progressive formation of crystalline clusters was observed, as revealed by sequential changes of SAED and dark field images and corroborated in the high resolution TEM images (HRTEM). The growth of crystalline clusters at the nanometer scale occurs without destruction of the nanoporous structures.

Introduction

Novel porous materials have attracted much attention [1] because of their wide-ranging potential applications in

D. E. Diaz-Droguett · V. M. Fuenzalida (✉) ·
M. S. Diaz-Espinoza
Departamento de Física, Facultad de Ciencias Físicas y
Matemáticas, Universidad de Chile, Av. Blanco Encalada 2008,
Santiago, RM 8370449, Chile
e-mail: vfuenzal@ing.uchile.cl

Present Address:
M. S. Diaz-Espinoza
Facultad de Cs. Naturales, Matemáticas y del Medio Ambiente,
Universidad Tecnológica Metropolitana, Santiago, Chile

G. Solorzano
Departamento de Ciência dos Materiais e Metalurgia, DCMM,
PUC-RIO, Rio de Janeiro, Brazil

catalysis and nanotechnology. On the other hand molybdenum trioxide MoO$_3$ is a promissory material because of its wide spectrum of potential applications in electronic display systems, solid state micro batteries and gas sensors. Moreover, MoO$_3$ is a widely used catalyst [2–4]. The catalytic properties can be controlled by varying the surface structure of the oxide or by changing the valence state of the molybdenum atoms [5]. In addition, molybdenum trioxide and molybdenum sub-oxides are of great interest in catalysis as a model system to elucidate the correlations between the structure and the catalytic performance [6]. It is worthwhile to note that MoO$_3$ is also a good precursor for the synthesis of many other important materials, such as MoS$_2$, MoSe$_2$, Mo, and host–guest compounds [7–11].

One way to synthesize MoO$_3$ nanoparticles is through the inert gas condensation process (IGC). The IGC method involves the physical evaporation of a material in the presence of a carrier gas at a pressure around 100 Pa [12]. At this pressure the mean free path is in the submillimeter range and the evaporated material cools down by colliding with the carrier gas molecules in its path, leading to nanoclusters collected onto a cold surface. The size of the nanoclusters depends on the evaporated material, the carrier gas and it pressure; lighter gases lead to the production of smaller particles [12, 13].

In this research the IGC method was used to generate molybdenum oxide nanostructures using hydrogen as carrier gas at pressures from 100 Pa to 600 Pa. The samples were characterized using X-ray photoelectron spectroscopy (XPS), X-ray powder diffraction (XRD), conventional transmission electron microscopy (TEM), selected area diffraction patterns (SAED) and high resolution transmission electron microscopy (HRTEM). The effect of the electron beam of the TEM on the amorphous MoO$_3$ nanostructures was also analyzed.

Experimental procedure

Experimental set up and synthesis of MoO_3 nanostructures by means of the IGC method

A high vacuum chamber was adapted to synthesize materials via the Inert Gas Condensation method in a controlled atmosphere. A turbomolecular pump backed by a rotary pump was used to reach a pressure of the order of 10^{-4} Pa, This is much lower than the working pressure and provides a clean background, particularly avoiding oxygen in the system, which has been shown to affect nanostructure growth [13]. A mass spectrometer is used to monitor the partial pressure of active gases, mainly O_2, N_2, H_2O and Ar; the latter is inert, but it can affect the growth because of its mass. After evacuating the chamber, the carrier gas is injected to reach the operation pressure, around 100 Pa. This pressure is maintained only with the rotary pump, in order to avoid excess gas flow.

A tungsten boat 95 mm in length, 10 mm wide and 0.1 mm thick is resistively heated until the working temperature is achieved. The temperature is measured with an optical pyrometer through a sapphire window. The nanomaterial is collected on the cold surface of a condenser consisting of a copper semi cylinder 152 mm external diameter, 3 mm thick and 300 mm long, cooled with liquid nitrogen. The tungsten boat is in the axis of the semi cylinder; around 75 mm from the internal surface of the condenser; this distance remains fixed for all the evaporations.

A simple scheme of the experimental setup is shown in Fig. 1.

In a typical experiment, a cold-pressed pellet of 0.5 g of MoO_3 is placed on the tungsten boat. MoO_3 was evaporated using hydrogen (AGA, 99.995%, $O_2 < 5$ ppm and $H_2O < 4$ ppm) in the pressure range from 100 Pa to 600 Pa
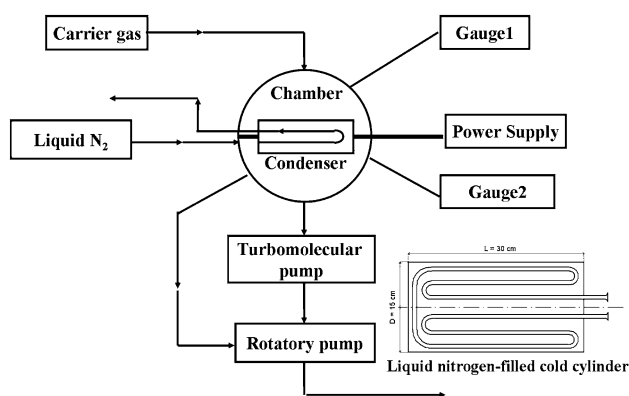
and source temperatures in the range from 720 °C to 1250 °C. Hydrogen in the exhaust line was diluted in nitrogen in order to reach a concentration below the flammability threshold.

Materials characterization

Surface chemical characterization of the samples was performed by a XPS Physical Electronics 1257 system. Crystallographic information was obtained with XRD using a Siemens D5000 diffractometer working with CuKα radiation of 0.15406 nm. The morphology and microstructure of the samples was examined with TEM/HRTEM JEOL 2010 instrument operating at 200 kV under diffraction and phase contrast modes.

Results and discussion

The preparation conditions of the MoO_3 nanomaterial by IGC are summarized in Table 1. The yields are variable and the amounts obtained were below 0.3 g in all the evaporations. Table 1 shows the morphologies of each sample, as revealed by TEM. The results were reproducible for each condition.

The evaporation of MoO_3 in hydrogen at source temperatures above 1000 °C always lead to amorphous nanoporous structures, whereas the evaporation below 750 °C always lead to crystalline nanostructures. The temperature range from 750 °C to 1000 °C generated a mixture of amorphous as well as crystalline nanoparticles, although at present it is not clear how this depends on other experimental parameters such as the pressure.

Characterization of the amorphous nanostructures

Chemical characterization

The XPS spectrum of a sample grown under condition 2 (100 Pa, 1196 °C) is depicted in Fig. 2, showing the $Mo3p_{1/2}$, $Mo3p_{3/2}$, $Mo3d_{3/2}$, $Mo3d_{5/2}$, Mo4p photoelectron peaks. No elements besides molybdenum, oxygen, and adventitious carbon were detected; in particular, there is no contamination with tungsten from the boat. The inset is a high resolution XPS spectrum of the Mo3d photoemission signal, which allows the identification of the oxide as MoO_3.

XRD analysis

Figure 3 is the XRD pattern of a nanoporous sample obtained under a hydrogen pressure of 400 Pa and the maximum source temperature used of 1057 °C. The

Fig. 1 Experimental set up for the synthesis of MoO_3 nanostructures by means of condensation in a carrier gas. The inset shows the dimensions of the condenser

Table 1 Evaporation parameters, yields and morphologies of MoO_3

Condition	Pressure hydrogen [Pa]	Maximum temperature [°C]	Yields (%)	Morphology
1	200	1222	54.8	Amorphous nanoporous
2	100	1196	52.7	Amorphous nanoporous
3	200	1161	65.6	Amorphous nanoporous
4	400	1057	40.2	Amorphous continuous
5	600	1023	35.0	Amorphous nanoporous
6	200	866	28.9	Amorphous nanoporous
7	200	743	14.3	Amorphous nanoporous
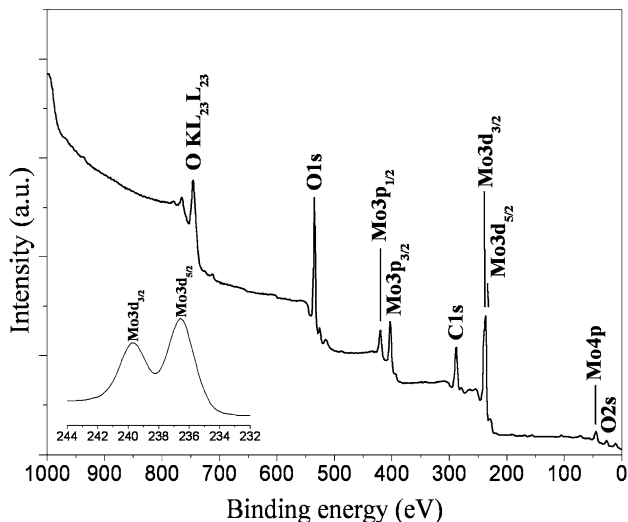
Fig. 2 XPS spectrum of a MoO_3 nanoporous sample obtained under condition 2 (100 Pa, 1196 °C)
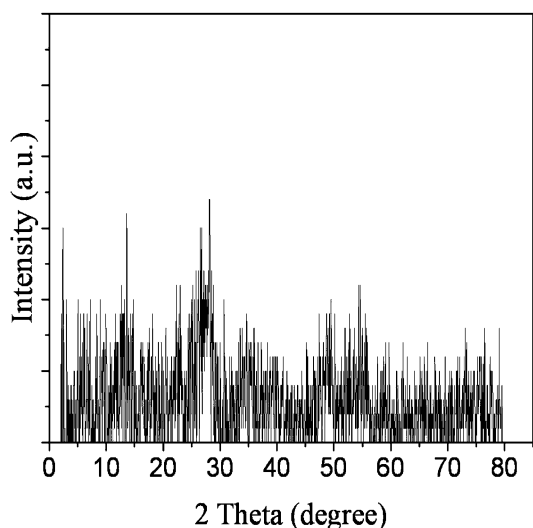
Fig. 3 XRD pattern of a MoO_3 nanoporous sample obtained under condition 4 (400 Pa, 1057 °C)

diffractogram does not define reflections, indicating the amorphous character of the sample, later corroborated by means of selected area electron diffraction (SAED) in the TEM.

### Morphological and structural characterization

TEM, HRTEM and SAED results of the as-received samples: Figure 4 shows the TEM images of a nanoporous structure grown under condition 1 (200 Pa, 1222 °C). Figure 4a and c are the dark and bright field images, respectively. The images show the porous character of the sample with porosity ranging from 10 nm to 85 nm. Figure 4c suggests that the sample consists of overlapped MoO_3 sheets or flakes. The inset 4b of Fig. 4 is a SAED showing a diffuse electron diffraction pattern, obtained after 1 min of exposure to the electron beam, indicating the initial amorphous character of the sample.

Figure 5 is a high magnification dark field image of a sample grown under condition 4 (400 Pa, 1057 °C). The inset 5a is a SAED showing again a diffuse pattern, thereby revealing the initial amorphous character of the sample. Under this synthesis condition the sample was non-porous as shown by the dark field TEM image (Fig. 5b).

In-situ crystallization induced by the electron beam: Figure 6 shows TEM images of the same sample described in Fig. 4, but after different electron beam irradiation times in the TEM. Figure 6a and b show the sequential changes in SAEDs. Figure 6a shows that after 10 min of irradiation well-defined rings and a few spots reveal the onset of crystallization. Figure 6b was recorded after 20 min; during the last 10 min the electron beam was concentrated onto an area of around 35 nm in diameter in order to generate a more intense effect. The higher definition of the diffraction rings indicates an increase in the number of crystallites with time.

Figure 6c is a dark field image recorded after the irradiation. The framed portion of this nanoporous structure, expanded in Fig. 6d, is the area strongly affected by the electron beam and shows some highly illuminated areas, identified as clusters of new crystallites due to the electron irradiation. It is worth noticing that these crystallites do not
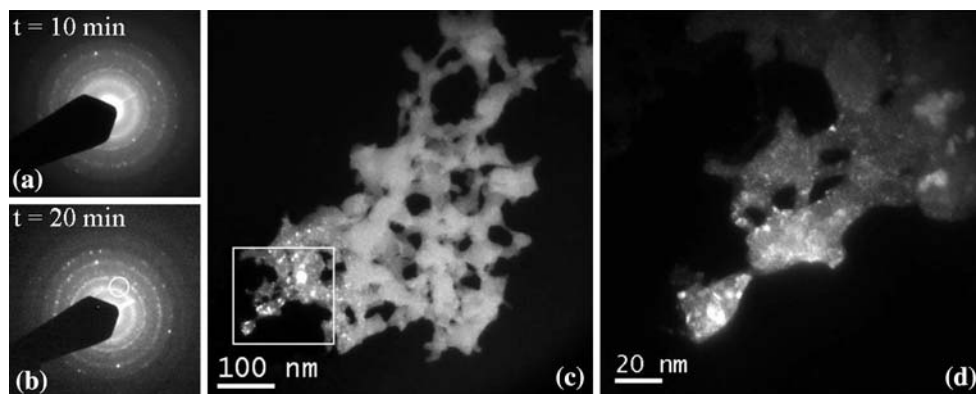
Fig. 4 TEM images of a sample grown under condition 1 (200 Pa, 1222 °C). (**a**) and (**c**) are dark field/bright field images obtained at the beginning of the TEM examination showing the porous character of the sample. (**b**) SAED showing a diffuse pattern
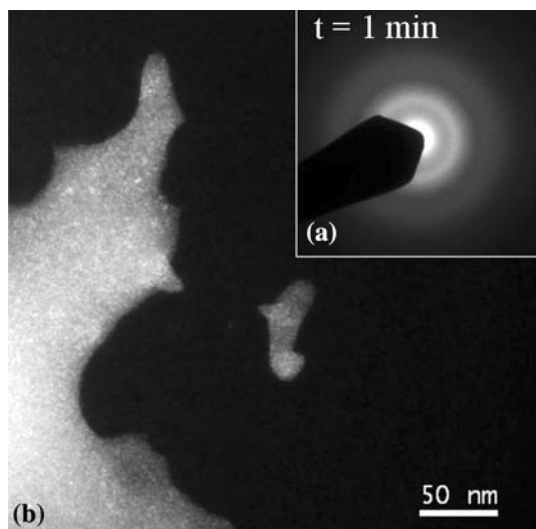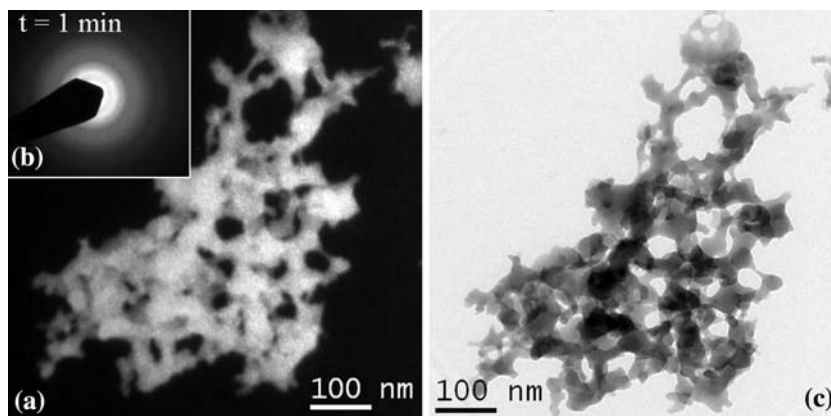
Fig. 5 TEM image of a sample grown under condition 4 (400 Pa, 1057 °C). The inset (**a**) is a SAED showing a diffuse pattern; (**b**) dark field TEM image

appear in the dark field TEM image of Fig. 4a, and that the growth of the crystalline clusters at the nanometer scale occurs without destroying the nanoporous structures.

Another example of the electron beam effects on the MoO_3 sample is shown in Fig. 7, corresponding to the TEM images of the sample shown in Fig. 5b, but now after a longer exposure to the electron beam. The starting electron pattern (Fig. 5a) was diffuse, corresponding to an amorphous material. After irradiation, this non-porous sample shows the same crystallization phenomenon under electron irradiation that the nanoporous samples exhibited, however at slower kinetics. After some minutes the irradiated zone shows clustering and the SAED indicates different crystallization degrees at different irradiation times, as is observed in Fig. 7a and b taken after 28 and 43 min of electron beam irradiation, respectively.

Figure 7c corresponds to the same area shown in Fig. 5b, but after electron irradiation. The image was generated using as illumination source the spots limited by the objective aperture in the diffraction ring indicated in the SAED of the Fig. 7b. This dark field TEM image shows the formation of crystalline clusters, a phenomenon corroborated by the HRTEM image of Fig. 7d, which displays the crystal lattice of the new crystalline domains, grown with different crystallographic orientations with an interplanar spacing of ~0.31 nm. The possibility of reduction of the starting oxide to metallic molybdenum is ruled out


Fig. 6 TEM images (**a**) and (**b**) are SAEDs showing the sequential changes of the electron diffraction patterns at different irradiation times, spot and ring formation suggesting formation of crystalline domains. (**c**) Dark field TEM image revealing the formation of crystalline clusters in the irradiated zone. (**d**) Enlargement of the part framed in (**c**)

Fig. 7 (**a**) and (**b**) are SAEDs revealing crystallization of the amorphous sample shown in the dark field TEM image of the Fig. 5b after been irradiated with electron beam. (**c**) Dark field TEM image showing the appearance of crystalline clusters. (**d**) HRTEM image of the framed zone in (**c**) showing crystal lattice of the new formed crystalline domains
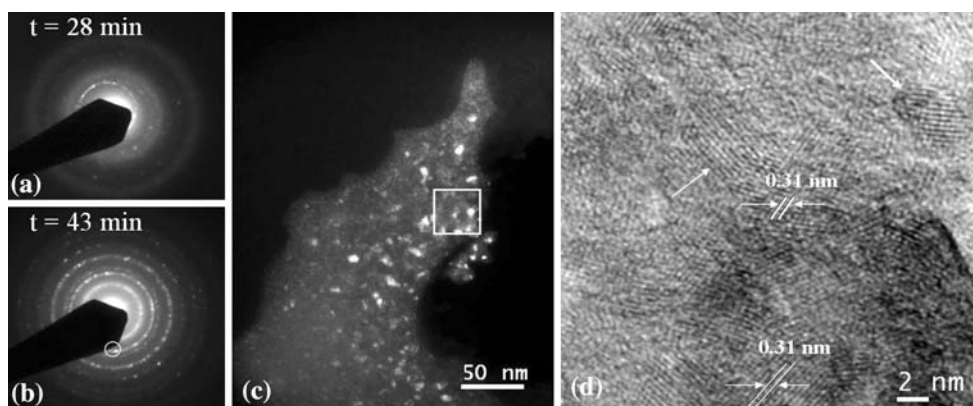
because the interplanar distance of 0.31 nm does not match any interplanar distance of molybdenum.

Several mechanisms can be responsible for the e-beam-induced crystallization, among them are local heating or other dynamic processes due to electron impact. We do not have quantitative data to compare the effects of the same electron dose delivered at high intensity and short time or at low intensity and longer times. However, qualitatively speaking, a prolonged observation of a large area does not induce the same crystallization than the concentrated beam on a small area, which supports the hypothesis of local heating. This is further supported by the fact that the crystallization is slower in the non-porous sample, in which heat dissipation is expected to be higher than in the porous samples, leading to a smaller local temperature increase. We believe that crystallization is associated with chemical changes due to oxygen loss. Figure 8 shows EDS spectra of a nanoporous sample before and after irradiation, with a change in the Mo:O intensities from 3.1 before irradiation to 5.7 after irradiation. This suggests oxygen loss, although we cannot provide a quantitative analysis or the stoichiometry of the crystallized material. The interplanar distance of 0.31 nm measured in Fig. 7d does not match the values of molybdenum metal or MoO_2, although it does match the separation between the (202) lattice planes of MoO_3.

In summary, we have shown that the preparation of MoO_3 under conditions very far from equilibrium originates nanoporous amorphous structures, which are far from equilibrium, too. One necessary condition to obtain these structures instead of crystalline nanoparticles is a MoO_3 partial pressure of at least one order of magnitude larger than the pressure of the carrier gas, which also means a large rate of supply of material (high evaporation rate); this parameter is controlled by the source temperature. A second necessary condition seems to be the quenching of the MoO_3 from the gas phase onto a cold surface at 77 K. It is yet unclear if the use of a reducing atmosphere is crucial for the process. The technique can be applied to other
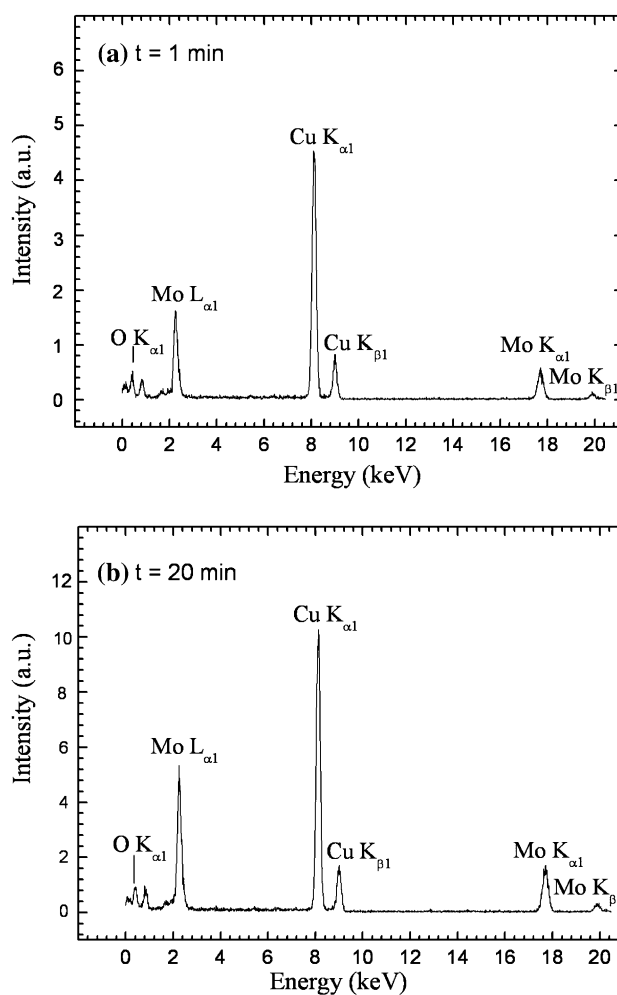
Fig. 8 EDS spectra of the nanoporous sample (**a**) taken at the beginning of the examination (after 1 min of electron beam irradiation) and (**b**) after 20 min of irradiation

materials of relatively high vapor pressure, such as SnO_2, which may find applications in sensors. Moreover, the material can be directly deposited on any substrate, provided that it is properly cooled to 77 K.

Conclusions

MoO$_3$ amorphous structures, porous and non-porous, were obtained by resistively evaporating MoO$_3$ in a hydrogen atmosphere at high MoO$_3$ evaporation rates, with source temperatures above 1000 °C. Evaporation at moderate temperatures did not lead to amorphous structures. The MoO$_3$ amorphous samples crystallize after a few minutes under the incidence of the electron beam of the TEM, forming nano-scale crystalline domains. The porosity of the nanoporous samples is in the range of 10–85 nm and is not disturbed by the crystallization process.

References

1. Kresge CT, Leonowicz ME, Roth WJ, Vartuli JC, Beck JS (1992) Nature (London) 359:710
2. Hussain Z (2001) J Mater Res 16:2695
3. Ferroni M, Guidi V, Martinelli G, Sacerdotti M, Nelli P, Sberveglieri G (1998) Sens Actuators B 48:285
4. Zeng HC (1998) Inorg Chem 37:1967
5. Wang S, Zhang Y, Wang W, Li G, Ma X, Li X, Zhang Z, Qian Y (2006) J Cryst Growth 290:96
6. Wang D, Su D, Schlögl R (2003) Cryst Res Technol 38(2):153 DOI 10.1002/crat. 200310018
7. Zach MP, Ng KH, Penner RM (2000) Science 290:2120
8. Margulis L, Salitra G, Tenne R, Talianker M (1993) Nature (London) 365:113
9. Hersfinkel M, Gheber LA, Volterra B, Hutchison JL, Margulis L, Tenne R (1994) J Am Chem Soc 116:1914
10. Feldman Y, Wasserman E, Srolouvitz DJ, Tenne R (1995) Science 267:222
11. Hagrman PJ, Hagrman D, Zubieta J (1999) Angew Chem Int Ed Engl 38:2638
12. Granqvist C, Buhrman R (1976) J Appl Phy 47(5):2200
13. Turker M (2004) Mater Sci Eng A 367:74